Journal of Colloid and Interface Science 239, 399–408 (2001)
doi:10.1006/jcis.2001.7620, available online at http://www.idealibrary.com on IDEAL®

$LiBr \cdot 2H_2O$ Crystallization Inhibition in the Presence of Additives

Terry Arthur Ring,[1] James A. Dirksen, Kristin Nicole Duvall, and Nathalie Jongen

Department of Chemical Engineering, University of Utah, 50 S Central Campus Drive, Salt Lake City, Utah 84112

Received August 3, 1999; accepted April 13, 2001

Experiments have been performed to measure the effect of additives on the crystallization temperature of concentrated LiBr solutions cooled at a rate of 20°C/h. The measured crystallization temperatures correspond not to the temperatures of equilibrium solubility but to the critical temperature for heterogeneous nucleation of the hydrated LiBr salt on the glass wall of the test tube containing the sample solution. Various additives at concentrations from 250 to 1500 ppm have been investigated. Some soluble additives further decreased the experimental crystallization temperature by as much as 13°C, corresponding to 22°C below the equilibrium solubility. Large decreases in the crystallization temperature can be correlated with large values of complexation constants of the additive for either the Li^+ or the Br^- ion in solution. Solution complexation, however, is not sufficient to explain the magnitude of the decrease in the crystallization temperature. The only phenomenon capable of quantitatively explaining the magnitude of the decrease in the crystallization temperature is the change in the crystal/solution interfacial energy due to adsorption of the additive on the surface of the prenucleation embryos. A quantitative model of the crystal/solution interfacial energy due to adsorption has been developed using both the Langmuir and Gibbs adsorption equations, allowing the quantitative prediction of crystallization temperatures with additive concentration.

Key Words: crystallization; crystallization temperature; lithium bromide; inhibition; additives.

INTRODUCTION

Concentrated LiBr solutions are used in absorption heat pumps for heating and cooling buildings. In this equipment water vapor, not Freon, is the working fluid used in compressive heat pumps (1). Water vapor is evaporated from a relatively dilute LiBr solution at high temperature and absorbed into a concentrated LiBr solution at low temperature. The concentrated LiBr solution from the multieffect evaporator is cooled in a heat exchanger to low temperatures near the crystallization temperature of the solution. As in any heat engine cycle, the Carnot efficiency (also called the "conversion factor") is given by difference between the high and low temperatures divided by the high temperature (2), $\eta = (T_H - T_L/T_H)$. Additives that inhibit crystallization provide an opportunity to expand the operating temperature range for LiBr absorption heat pumps and thus their efficiency.

The crystallization point of concentrated LiBr solutions depends upon their concentration, since different solids (e.g., ice, tri-, di-, and monohydrates of LiBr) are produced according to the concentration of the LiBr solution. When cooled, a concentrated LiBr solution—like all particulate-free salt solutions—does not crystallize at the equilibrium crystallization temperature, but below the equilibrium crystallization temperature, due to the need to supersaturate the solution before nucleation can take place. This range of temperature is called the Ostwald–Meyers metastable zone. Each type of solution has a different width for its metastable zone.

Our previous paper (3) showed that the onset of LiBr salt nucleation was detected by a 0.4°C deviation from the theoretical cooling curve that does not consider a phase change. Nucleation occurred as surface nucleation on the Pyrex glass surface. The observed crystallization temperatures for various LiBr solution concentrations were predicted using the classical nucleation theory whose most useful equations are reviewed below. The objective of this paper is to expand this approach to include the effect of additives.

The driving force for nucleation is the saturation ratio defined as the ratio of the actual solution concentration when crystallization takes place to the equilibrium concentration, $S = C/C_{eq}$. When the saturation ratio is greater than 1.0, the solution is supersaturated with respect to the solid. Supersaturation in this case is due to supercooling, $T - T_{eq}$, in the solution and is given as

$$S = \exp\left[\left(\frac{\Delta H_f}{R_g T_{eq}}\right)\left(\frac{T - T_{eq}}{T}\right)\right], \qquad [1]$$

where ΔH_f is the heat of crystallization of the crystallizing solid, T is the actual temperature of crystallization, T_{eq} is the equilibrium solubility temperature, and R_g is the gas constant.

Using the concept of the critical supersaturation, S_c, which is defined as the value of S necessary to give a nucleation rate which is observable experimentally, (1 nucleus $\cdot$ cm^{-2} $\cdot$ min^{-1} for surface nucleation), the classical surface nucleation

[1] To whom correspondence should be addressed.

0021-9797/01 $35.00

equation,

$$I_s\left[\frac{\#}{\text{cm}^2\text{min}}\right] = \left.\frac{dN(r)}{dt}\right|_{r=r_s^*}$$

$$= 4\mathbf{D}N_0 r_s^* N_o \hat{V}^{1/3} \exp\left[\frac{-\Delta G_s(r_s^*)}{k_B T}\right] \quad [2]$$

$$= 4\mathbf{D}N_0 \frac{\gamma_\varepsilon \beta_L \hat{V}^{2/3}}{\beta_A R_g T \ln(S)} N_0 \hat{V}^{1/3}$$

$$\times \exp\left[\frac{-\left(\frac{\gamma_\varepsilon^2 \beta_L^2 \hat{V}^{2/3}}{2\beta_A R_g T \ln(S)}\right)}{k_B T}\right], \quad [3]$$

with

$$r_s^* = \frac{\gamma_\varepsilon \beta_L \hat{V}^{2/3}}{\beta_A R_g T \ln(S)},$$

was used to determine a critical supersaturation that is responsible for these experimentally observable nucleation rates. In the above equations, **D** is the solution diffusion coefficient, N_0 is the number concentration of LiBr in solution, r^* is the critical radius for homogeneous nucleation (subscript s is for surface nucleation), γ is the surface energy for the crystal/solution interface, $\gamma_\varepsilon[\approx \gamma \cdot d]$ is the edge energy per unit length, and d, the center-to-center distance of two LiBr $\cdot n\text{H}_2\text{O}$ molecules, is related to the molar volume, $\hat{V}$, of the crystal ($d = \hat{V}^{1/3}$). β_v and β_a are the volume and area conversion factors for homogeneous nucleation (for spherical nuclei, $\beta_v = 4\pi/3$ and $\beta_a = 4\pi$; for cubic nuclei, $\beta_v = 1$ and $\beta_a = 6$), β_L is the edge length conversion factor, β_A is the surface area conversion factor for surface nucleation (for a cylindrical embryo of height $d/2$ above the surface, $\beta_A = \pi$ and $\beta_L = 2\pi$; for a cubic embryo with an effective radius $= L/2$, $\beta_A = 1$ and $\beta_L = 4$), and k_B is Boltzmann's constant.

Using the surface nucleation theory, the experimental crystallization temperatures could be derived in agreement with experimental observations when a crystal/solution interfacial surface energy of 40.0 ± 1.2 erg/cm^2 was used (3).

The objective of the present work is to investigate the effect of additives on the crystallization of hydrated LiBr salts. Additives can inhibit or accelerate the nucleation depending on their properties. Insoluble additives provide heterogeneous seeds for nucleation to take place at lower supersaturation levels near the equilibrium solubility, increasing the nucleation rate. Active additives, forming very stable complexes with the species involved in the crystallization reaction, decrease the nucleation rate by diminishing the activity in solution of these species: The more stable the complex, the larger the inhibition. Another inhibitor effect can come from a structural matching between the additive and the solid. Sarig and Kahana (4) highlighted this phenomenon by showing the inhibitory effect of poly(glutamic acid), with distances between carboxylate groups around 8 Å, on the precipitation of $CaSO_4 \cdot 2H_2O$, with intercationic distances of about 8.1 Å.

Additives in crystallization are the subject of much recent work in the literature. A 1995 book by Nyvlt and Ulrich (5) titled *Admixtures in Crystallization* qualitatively discusses the effect additives have in various aspects of crystallization and gives 195 pages of tables identifying the effect (e.g., nucleation, crystal growth, crystal habit, crystal size, and distribution of additive in crystal) that various additives have on the crystallization of 287 different salts. Unfortunately, hydrated LiBr salts are not part of this compilation. An interesting quote from this book is "a consistent theory of the effect of admixtures on individual aspects of the process of crystallization is still missing." This book also speculates under a heading Heterogeneous Nucleation that:

> Surface active substances deactivate heterogeneous particles and thus increase the width of the metastable region (6–7). The extent of this action is given by the amount and catalytic activity of foreign particles. An opposite influence (8–9) can be explained by the fact that surface active substances decrease the surface energy so that the nucleation rate can increase. The shape of the curve of nucleation rate vs. the admixture concentration resembles the adsorption isotherms of surface active substances on solid surfaces so that there may be expected a direct link of nucleation rate rise with the adsorption of the admixture on the surface.

The 1996 book *Crystal Growth of Organic Materials*, edited by Myerson *et al.* (10), contains several articles from a 1995 symposium. Articles of interest are one by Niehorster *et al.* (11) on the modeling of the effect of an additive on crystal habit modification and another by Sun and Myerson (12) on the effect of an additive on nucleation. Molecular modeling of the attachment energy for additives at various crystal surfaces has been performed and the effect of this change in attachment energy for the various crystal surfaces has been used to predict the new crystal habit.

The 1998 book *Water Soluble Polymers–Solution Properties and Applications* edited by Amjad contains an article from a 1997 symposium by He *et al.* (28) that gives a semiempirical model of crystallization inhibition. In this work the classical nucleation equation (Gibbs–Kelvin equation) for the logarithm of the induction time is used. Additives are assumed to effect the nuclei's physicochemical properties such as the surface energy, the shape factor, and the wetting angle. All of these properties, to their appropriate powers, are lumped into a single parameter, which is set to be proportional to the concentration of the additive. In this way the effect of additive on induction time is predicted and compared to experiment. For several of the additives investigated, the lumped parameter is linear; however, for several effective additives the concentration dependence is nonlinear. For those cases, a polynomial curve fit is used to fit the induction time data. In a 1999 Internet article, Ferguson (29) uses the same approach as He *et al.* but suggests a power law dependence of the induction time on additive concentration.

In the present work, the effects of additives and their concentrations on the crystallization temperature of LiBr solutions were measured and compared to predictions of the crystallization

TABLE 1
List of Additives Used

Methylenediphosphonic acid[a]	MDPA	$CH_6P_2O_6$	98%
Pyrophosphoric acid[a]	PPA	$H_4P_2O_7$	Technical grade
Aminotri(methylene phosphonic acid)[b]	ATMP	$N(CH_2PO_3H_2)_3$	Dequest 2000
Diethylenetriaminepenta(methylene phosphonic acid)[b]	DTPMP	$CH_2PO_3H_2N(C_2H_4N(CH_2PO_3H_2)_2)_2$	Dequest 2060
1-Hydroxyethylidene-1,1-diphosphonic acid[b]	HEDP	$CH_3C(OH)(PO_3H_2)_2$	Dequest 2010
5-Amino-2,4,6-trioxo-1,3-perhydrodizine-*N*,*N*-diacetic acid[c]	Uramil-*N*,*N*-diacetic acid	$C_8H_9O_7N_3$	>99.0%
Polyphosporic acid[c]	PolyPA	$H(PO_3H)_nOH$	
Potassium iodate[a]		KIO_3	>99.0%
Malic acid[d]		$C_4H_6O_5$	
Malonic acid[a]		$C_3H_4O_4$	99%
Phosphoric acid[c]		H_3PO_4	85.5%
Adenosine 5′-(trihydrogendiphosphate)[f]	ADP	$C_{10}H_{15}N_5O_{10}P_2$	
Ethylenediaminetetraacetic acid[c]	EDTA	$C_{10}H_{16}O_8N_2$	>99.0%
Potassium ferrocyanide[g]		$K_4Fe(CN)_6$	>99.0%
Adenosine 5′-(tetrahydrogentriphosphate)[f]	ATP	$C_{10}H_{16}N_5O_{13}P_3$	
Potassium bromate[h]		$KBrO_3$	99.8%
Zinc bromide[d]		$ZnBr_2$	>99.99%
N-Methyl formamide[i]		HCO-NH-CH_3	>99.8%
Potassium bromide[d]		KBr	>99.99%
Thallium chloride[a]		$TlCl_3$	
Triton X-100[j]		$C_{34}H_{64}O_{11}$ on average	
Potassium iodide		KI	
Cadmium chloride[a]		$CdCl_2$	>99.0%
Ethylene glycol[c]		CH_2OH-CH_2OH	
4,7,13,18-Tetraoxa-1,10-diazabicyclo[8.5.5]eicosane[a]	Eicosane	$C_{14}H_{28}N_2O_4$	98%
Indium chloride[a]		$InCl_3$	98%
18-Crown-6 ether[a]		$C_{12}H_{24}O_6$	99%

[a] Aldrich, Milwaukee, WI 53233.
[b] Monsanto, St Louis, MO 63167.
[c] Paltz & Bauer Inc., Waterbury, CT 06708.
[d] J. T. Baker, Phillipsburg, NJ 08865.
[e] Mallinckrodt Inc., Paris, KT 40361.
[f] ICN Biomedicals, Inc., Aurora, OH 44202.
[g] Kodak, Rochester, NY 14650.
[h] Merck, Inc., Rahway NJ.
[i] Sigma, St. Louis, MO 63178.
[j] Spectrum Chemical, Gardena, CA 90248.

temperature using the effect of adsorption of the soluble additives on the energy of the heterogeneous surface. In addition, molecular modeling was carried out to predict the critical parameters of the additive adsorption from solution.

EXPERIMENTAL METHOD

Concentrated stock LiBr solutions were prepared by mixing analytical reagent grade LiBr (Aldrich) with doubly distilled deionized water and filtering the solution through a 0.2-μm Millipore filter. The concentrations were validated by measuring the specific density of the solution and the index of refraction and comparing with standard tables (13, 14). The sensitivity of these two techniques has been established as ±0.2 wt% for picnometry and ±0.3 wt% for refractive index. The values quoted for LiBr concentrations are the average values determined using these two methods. The concentrations of LiBr in the solutions used were 60.54 and 60.82 wt%.

Test tubes were filled with 25 mL of a concentrated LiBr solution taken from a stock solution. Small quantities of additives (listed in Table 1) were added to some of them (typically 500 mol ppm based upon LiBr and water). The tubes were then placed in a temperature-programmable cooling bath. The bath could hold 16 test tubes. The LiBr solutions were individually monitored for the solution temperature allowing crystallization point statistics to be obtained. The 16 sample vials contained within the refrigerated temperature bath were divided into four separate quadrants. Three quadrants contained stock solutions with ppm levels of various dopants and one quadrant contained the control samples. The control samples consisted of one vial of deionized water and three LiBr stock solution vials. These test tubes were then sealed and heated for 24 h at 50°C to ensure solubilization of the LiBr solutions. End-over-end agitation was used to ensure uniform composition of the solution. If the additive was not completely dissolved in the LiBr solution, the test tube with that additive was rejected. After solubilization was ensured, the test tube was cooled at a ramp of 20°C/h. Inside the test tube a thermal well with a thermocouple of precision ±0.01°C recorded the temperature of the solution as a function of time using computerized data logging equipment. The bath temperature was

undergoing a ramped decrease in the set point, as presented in a previous paper (3): excellent fits with errors less than ±0.1°C were obtained. When the solution crystallized, the heat of crystallization was released and the temperature of the solution increased slightly.

RESULTS AND DISCUSSION

An example of the cooling curves for various samples is given in Fig. 1. The crystallization points for the tested additives are easily identified by the deviation of the temperature from the cooling curve of a blank solution. This blank solution has a cooling curve that is easily predicted by a continuation of the nearly linear cooling curve of the solution above the crystallization point to temperatures below the crystallization point. The mathematical derivation of the sample cooling curve was derived previously (3). Experimental results of the minimum of the temperature curve for various solutions containing soluble additives are given in Table 2. It should be noted that the crystallization from pure LiBr solution starts on either the curved bottom of the test tube or the glass thermo well hanging into the top of the liquid at the center of the test tube and continues until the test tube is approximately 3/4 filled with large (0.5 × 8 cm) plate-like crystals. The crystals are lithium bromide dihydrate, $LiBr \cdot 2H_2O$, according to the literature (15) and verified using X-ray diffraction. When some additives are present (e.g., uramil–*N*,*N*-diacetic acid), the crystal habit is drastically modified to small needles which are up to 5 mm long and 1 mm in diameter.

Our concern is the identification of the additives inhibiting LiBr crystallization and the determination of their mechanism of action. Crystallization inhibition can take place following several mechanisms, including the decrease of the crystallization driving force, i.e., supersaturation; the increase of the critical

TABLE 2
Crystallization Temperatures Measured for Soluble Additives Behaving as "Crystallization Inhibitors"

Additive	LiBr concn (wt%)	Additive concn (mol ppm[a])	Crystallization temperature T_{min} ± SD (°C)
MDPA	60.54	250	−10.16 ± 3.17
PPA	60.82	500	−8.52 ± 4.17
ATMP	60.82	500	−8.24 ± 2.25
DTPMP	60.82	500	−6.67 ± 6.79
HEDP	60.82	500	−6.15 ± 7.49
Uramil–*N*,*N*-diacetic acid	60.54	500	−5.69 ± 2.92
PolyPA	60.82	500	−4.73 ± 3.72
KIO_3	60.54	250	−4.31 ± 0.70
Malic acid	60.54	500	−2.28 ± 3.61
Malonic acid	60.54	500	−2.09 ± 5.46
H_3PO_4	60.54	500	−1.96 ± 5.79
ADP	60.82	250	−1.05 ± 2.32
EDTA	60.54	500	−1.05 ± 2.92
$K_4Fe(CN)_6$	60.54	500	−0.01 ± 0.03
ATP	60.82	250	−1.05 ± 2.92
$KBrO_3$	60.54	575	0.40 ± 0.35
$ZnBr_2$	60.54	500	2.50 ± 0.39
N-Methyl formamide	60.54	500	2.68 ± 0.28
KBr	60.54	589	2.75 ± 0.88
$TlCl_3$	60.82	500	3.17 ± 0.41
Triton X-100	60.54	500	3.26 ± 0.26
KI	60.54	610	3.45 ± 0.29
$CdCl_2$	60.82	500	3.83 ± 0.38
Ethylene glycol	60.82	500	4.17 ± 0.53
Eicosane	60.82	500	4.23 ± 1.44
$InCl_3$	60.82	500	4.31 ± 0.23
18-Crown-6	60.82	500	5.86 ± 1.18
None	60.54	—	3.30 ± 0.44
	60.82†		4.38 ± 0.59

[a] Moles of additive per mole of LiBr on a ppm basis.

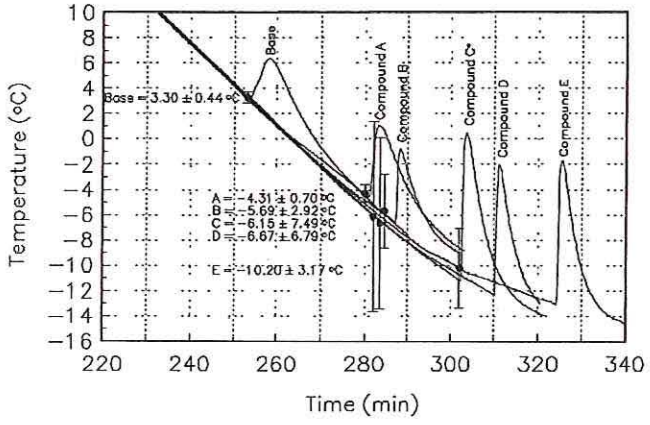

FIG. 1. Cooling curves of 60.54 wt% LiBr solutions with various additives. The peaks in temperature are caused by the release of the heat of crystallization when the solution starts to crystallize. The minimum in the curve to the left of the peak is the crystallization temperature measured experimentally. Additive concentrations are (A) 500 ppm KIO_3, (B) 500 ppm uramil–*N*,*N*-diacetic acid, (C) 500 ppm HEDP, (D) DTPMP, (E) 500 ppm MDPA.

supersaturation for nucleation; and the decrease of the crystal growth rate. This paper concentrates on the first two effects.

A soluble additive is able to influence the LiBr solubility by being a ligand for either Li^+ ions in solution or Br^- ions in solution. The effects of ligands for Li^+ ions in solution are discussed first.

Effect of Li^+ Ion Ligand Complexation

The solubility product of $LiBr \cdot 2H_2O$ is defined by the equation (3)

$$K_{sp} = [Li^+][Br^-][H_2O]^2,$$

where [ ] is the activity of a species in solution. The previous paper (3) explains that this solubility product accounts for the activity of water in solution. Knowing the solubility product of $LiBr \cdot 2H_2O$, we can determine the effect of a soluble Li^+ ion ligand by accounting for the loss of Li^+ ion activity due to

TABLE 3
Experimental Crystallization Temperature of 60.54 wt% LiBr Solution with Various Additives

Additive	Concentration (mole ppm)	Crystallization temperature (°C)	log K
None	0	+3.23±0.41	—
$KBrO_3$	575	+0.40±0.435	−0.82
H_3PO_4	500	−1.96 ± 5.879	0.95
Malic acid	500	−2.33 ± 3.61	1.0
KIO_3	250	−4.31 ± 0.70	1.1
EDTA	500	−1.11 ± 2.92	2.79
Uramil–*N*,*N*-diacetic acid	500	−5.77 ± 2.92	5.61

Additive complexation constant, $K = [LiA]/[Li^+][A^-]$.

complexation according to the equilibrium

$$iLi^+ + jB^{-b} \overset{K}{\leftrightarrow} [Li_iB_j]^{i-bj} \quad \text{with} \quad K = \frac{[Li_iB_j]^{i-bj}}{[Li^+]^i[B^{-b}]^j}, \quad [4]$$

where B^{-b} is the ligand with a charge $-b$. The Li^+ complexation equilibrium constants can be obtained from the literature (21–27). This complexation reaction results in a lower effective Li^+ concentration in solution and thus decreases the crystallization temperature. The larger the complexation constant, the more the crystallization temperature decreases. A set of experiments using this concept has been performed and the crystallization temperature of LiBr solutions with various additives have been measured. The results, given in Table 3, are plotted in Fig. 2. From these data, we see that the crystallization temperature generally decreases by more than 5°C as the Li^+ complexation constant K increases. The error bars are substantial in several cases suggesting that the correlation is not simply associated with the value of K but with other properties of the ligand.

We can in fact predict the effect of the ligand on the crystallization temperature of the solution. This is done by using the complexation equilibrium which lowers the effective Li^+ ion concentration in solution. Once the free Li^+ ion concentration is calculated, it can be used with the unaffected free Br^- ion concentration and the solubility product to determine the new equilibrium solubility of the solution. With this new equilibrium crystallization point, the surface nucleation theory is used to determine the new crystallization temperature due to surface nucleation. As shown in Fig. 3, the presence of the additives decreases the equilibrium solubility temperature and the crystallization temperature due to surface nucleation from its original value to a value about 0.2°C lower as the value of the log K is increased. Comparing these calculated results in Fig. 3 to the experimental results in Table 2, we see that the data for each of the additives are not well predicted by this model: 3.44°C (calculated) versus 0.4°C (measured) for log $K = -0.82$, 3.0°C versus −1.11°C for log $K = 2.79$, and 3.0°C versus −5.77°C for log $K = 5.61$.

As a result of this inconsistency between experiment and theory, we must consider that the decrease in supersaturation alone cannot explain the results. Thus we must consider that the surface energy of the crystal and/or embryo in the saturated solution is also altered by the presence of additives, which adsorb on the crystal surfaces. Drastic changes have been observed experimentally in crystal habit from large platelets to small crystallite needles with the addition of uramil–*N*,*N*-diacetic acid at 500 ppm and above. This observation indicates that the surface energy of the crystal faces has been altered drastically by this additive. In the calculation of the crystallization temperature due to surface nucleation, the surface energy plays an important role, as will be discussed later. An increase in the surface energy of 10 erg/cm^2 is sufficient to decrease the crystallization temperature by several degrees centigrade. Our difficulty at the moment is in predicting the new surface energy that an additive at a particular concentration would cause. Thus we can conclude that the effect of additives which complex Li^+ ions is twofold: (i) to decrease the amount of Li^+ ion in solution which according to prediction decreases the crystallization temperature by about 0.2°C; and (ii) to alter the surface energy of the crystal in solution. Considering the experimental results in Table 2, the second effect is the dominant effect.

Effect of Br^- Ion Ligand Complexation

In addition, some additives are able to complex the Br^- ion. The complexation constants for the Br^- ion can also be obtained

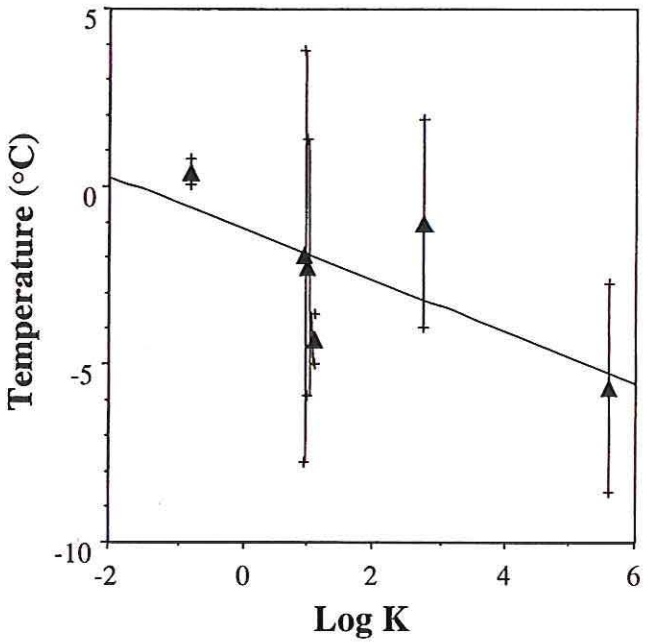

FIG. 2. Crystallization temperature of 60.54 wt% LiBr solutions with various additives plotted against the values of their Li^+ ion–ligand equilibrium constants. Data from Table 3. Error bars reflect the standard deviation of the crystallization temperatures measured.

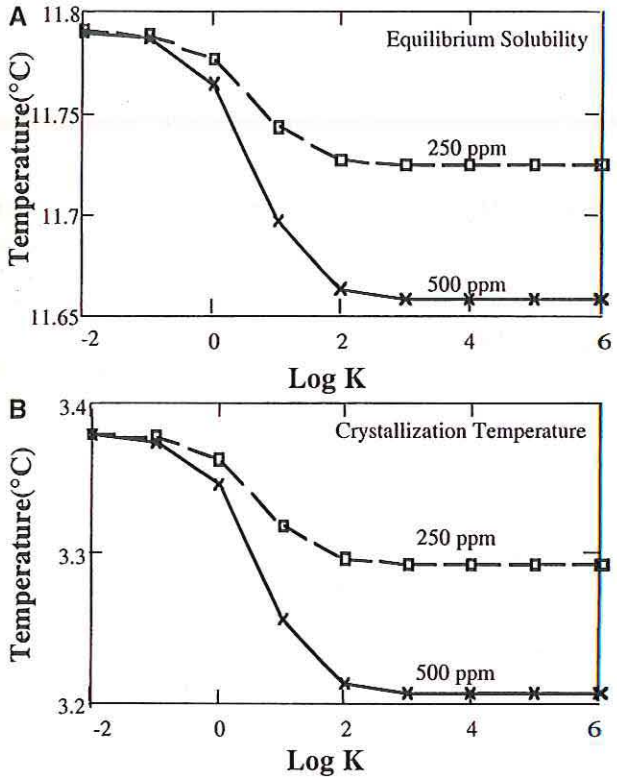

FIG. 3. (A) Equilibrium solubility of 60.54 wt% LiBr solution as functions of logarithm of the Li^+ ligand equilibrium constant, Log K, for two additive concentrations, (×) 500 mol ppm and ([ ]) 250 mol ppm. (B) Crystallization temperature of 60.54 wt% LiBr solution for surface nucleation as a function of logarithm of the Li^+ ligand equilibrium constant, Log K, for two additive concentrations, (×) 500 mol ppm and ([ ]) 250 mol ppm.

from the literature (24). These ligands are typically metal ions. In this case, we find that any ligand has one or more complexation equilibria of the form

$$M^{+m} + jBr^- \overset{K_{i,j}}{\leftrightarrow} MBr_j^{+(m-j)} \qquad [5]$$

$$\text{with} \qquad K_{1,j} = \frac{[MBr_j^{+(m-j)}]}{[M^{+m}][Br^-]^j},$$

where M^{+m} is the metal ion ligand of valence $+m$ and $MBr_j^{+(m-j)}$ is the bromine compound of valence $(m - j)$. Because there is often more than one complex of the type $MBr_j^{+(m-j)}$ in solution, e.g., $j = 1, 2, 3, 4, 5$, and 6, the effect of Br^- ion complexation is more powerful than the complexation of Li^+ ions. The nomenclature for $K_{i,j}$ is to use the complex formula $M_iBr_j^{+(mi-j)}$ where $i = 1$. To calculate the effect of this complexation, however, is more difficult. The final concentration of Br^- ion, after complexation due to the addition of $[M]_{Tot}$ moles of a ligand, is determined by solving two simultaneous equations with two unknowns, $[M^{+m}]$ and $[Br^-]$. The concentrations of these ions after equilibration of the solution are

$$[M]_{Tot} = [M^{+m}] + \sum_{j=1}^{j_{max}} K_{1,j}[M^{+m}][Br^-]^j \qquad [6]$$

$$[Br^-]_{Tot} = [Br^-] + \sum_{j=1}^{j_{max}} jK_{1,j}[M^{+m}][Br^-]^j. \qquad [7]$$

The value of $[Br^-]$ is the final concentration of Br^- ion when equilibrium is reached, which can be used with the unaffected Li^- ion concentration and the solubility product to determine the new crystallization temperature of the solution. A plot of the effect of metal additive concentrations of Cs^{+1}, Sn^{+2}, Cd^{+2}, Tl^{+3}, and Pd^{+2} on the equilibrium solubility and the crystallization temperature due to surface nucleation is shown in Fig. 4. Here we see that the effect is linear with the concentration and the most effective additives in decreasing the equilibrium solubility and crystallization temperature are the Pd^{+2} and Tl^{+3} ions. This is due to the strong complexing capabilities of the Pd^{+2} and Tl^{+3} ions for the Br^- ion (Pd^{+2}—log $K_{1,1} = 5.17$, log $K_{1,2} = 9.42$, log $K_{1,3} = 12.7$, log $K_{1,4} = 14.9$; Tl^{+3}—log $K_{1,1} = 8.9$, log $K_{1,2} = 16.4$, log $K_{1,3} = 22.1$, log $K_{1,4} = 25.7$ compared to Cs^{+1}—log $K_{1,1} = 0.03$ or Sn^{+2}—log $K_{1,1} = 0.88$, $K_{1,2} = 1.43$, log $K_{1,3} = 1.5$, log $K_{1,4} = 1.0$ (24)). Since there

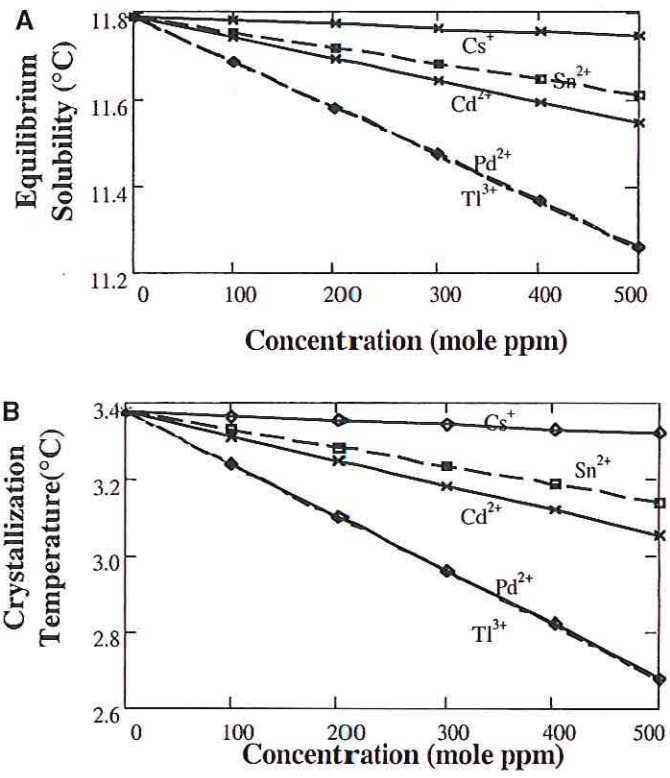

FIG. 4. (A) Equilibrium solubility of 60.54 wt% LiBr solution as a function of the concentration of the Br^- ligands. (B) Crystallization temperature of 60.54 wt% LiBr solution for surface nucleation as a function of the concentration of the Br^- ligands.

are multiple equilibria of the type $MBr_j^{+(m-j)}$, the Br^- ion complexes are more effective in reducing the crystallization temperature. However, this reduction is still small, i.e. $<0.8°C$ for 500 mole ppm Pd^{+2} or Tl^{+3} ions. The effect on the crystallization temperature of the Zn^{+2} ion, which is also a Br^- ion ligand, was experimentally measured to give a small 0.6°C decrease in the crystallization temperature. Prediction of the effects of Zn^{+2} on the lowering of the crystallization temperature is similar to that of Cs^+ ion, since the complexation constant is of similar magnitude. Therefore 500 ppm Zn^{+2} should give a decrease in the crystallization point and the crystallization temperature of 0.2°C, as shown in Fig. 4. Again, the experimental results in Table 2 show larger reductions in the crystallization temperature than predicted for Zn^{+2} addition. Therefore, we must consider that we have missed an important effect in predicting the crystallization temperature. Again, one possible explanation is that the surface energy of the crystal in the saturated solution is also altered by the addition of additives, which adsorb on the crystal surfaces.

Effect of Additives on the Crystal/Solution Interfacial Energy

To explain the experimental results, we must discuss the effects of these additives on the surface energy of the crystal in solution. The Li^+ ion and Br^- ion ligand complexes will also play a role in complexing the surface of $LiBr \cdot 2H_2O$ crystals and altering the surface energy of the $LiBr \cdot 2H_2O$/solution interface. The effect of the surface energy on the crystallization temperature due to surface nucleation is plotted in Fig. 5. The crystallization temperatures were calculated by inverting Eq. [3] for several surface energy values and assuming that I_s, the nucleation rate, equals 1 nucleus $\cdot$ cm^{-2} $\cdot$ min^{-1} and the LiBr concentration is 60.54 wt%.

Here we see that an increase in the crystal/solution interfacial energy from zero to 90 erg/cm^2 gives a 50°C decrease in the crystallization temperature. In this range of interfacial energies there are several well-established values: (a) 0 erg/cm^2, the value if seed crystals of the same material are present in sufficient numbers for nucleation sites; (b) 29 erg/cm^2, the surface energy of the ice/water interface (16); (c) 40 erg/cm^2, the value of the best fit (using Eq. [3] with $I_S = 1\#/cm^2s$) of the experimental crystallization temperature of $LiBr \cdot 2H_2O$ without additive, (d) 61 erg/cm^2, the value of the best fit (using Eq. [3] with $I_S = 1\#/cm^2s$) of the experimental crystallization temperature (i.e. $-5.69 \pm 2.92°C$) of $LiBr \cdot 2H_2O$ with 500 ppm uramil–*N*,*N*-diacetic acid additive; and (e) 90 erg/cm^2, the value of the solution/air interface at these LiBr concentrations (17). This is in good agreement with our experimental observations, as seen by comparing Fig. 5 to Table 2. Directly measuring this energy experimentally is very difficult and has not been done under crystal growth conditions in any systems that we are aware of. Nonetheless computational means are possible if the adsorption isotherm can be established and the analogy to the Gibbs adsorption equation can be used.

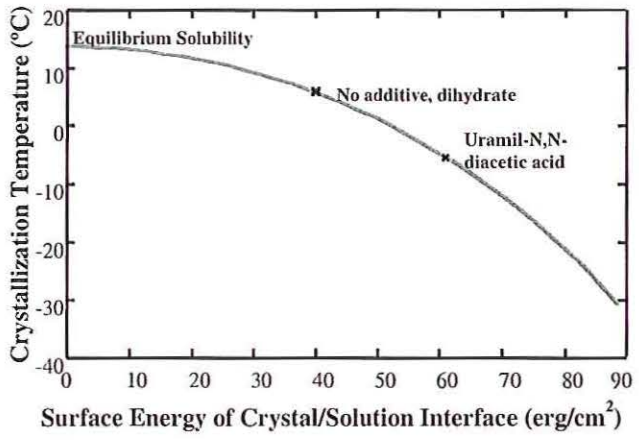

FIG. 5. Crystallization temperature due to the surface nucleation versus crystal/solution interfacial energy. The curve is the best fit of the experimental crystallization temperatures observed without additive and with 500 ppm uramil–*N*,*N*-diacetic acid.

The crystal/solution interfacial energy is altered by additive adsorption according to the Gibbs adsorption equation (18),

$$\Gamma_a^{(l)} = \frac{-1}{R_g T}\left(\frac{d\gamma_s}{d(\ln a_a)}\right), \qquad [8]$$

where $\Gamma_a^{(l)}$ is the adsorbed amount, γ_s is the crystal/solution interfacial energy, and a_a is the solution activity of the surface ligand or additive in our case. As derived by Gibbs, the above equation relates the surface energy of the liquid/air interface to the adsorbed amount given by the adsorption isotherm. We will use this same equation for the solid/liquid interface and use it to relate the effect of the crystal/solution interfacial energy to the adsorbed amount, $\Gamma_a^{(l)}$, if it is either experimentally measured or predicted by the Langmuir adsorption isotherm given by

$$\Gamma_a^{(l)} = \Gamma_m \frac{K_{Langmuir}\, a_a}{1 + K_{Langmuir}\, a_a}, \qquad [9]$$

where Γ_m is the adsorbed amount at monolayer coverage and $K_{Langmuir}$ is the adsorption equilibrium constant.

To obtain $\gamma = f(a_a, T)$, Eq. [8] is transformed into

$$-d\gamma_s = \frac{\Gamma_a^1 R_g T}{a_a}\, da_a. \qquad [10]$$

$\Gamma_a^{(l)}$ is then substituted from [9] into [10] and integrated to give

$$\int_{40}^{\gamma} -d\gamma_s = \int_0^{a_a} \Gamma_m R_g T \left(\frac{K_{Langmuir}}{1 + K_{Langmuir}\, a_a}\right) da_a, \qquad [11]$$

resulting in

$$\gamma_s = \Gamma_m R_g T \ln(1 + K_{Langmuir}\, a_a) + 40 \text{ erg/cm}^2. \qquad [12]$$

TABLE 4

Effects of Additive Concentration on the Crystallization Point of 60.82 wt% LiBr Solutions

Additive	Additive concentration (mole ppm[a])	Crystallization temperature $T_{min} \pm$ Std. Deviation (°C)
None	0	4.65 ± 0.56°C
MDPA	50	−4.80 ± 3.67°C
	150	−2.63 ± 5.11°C
	250	−8.88 ± 3.17°C
ATMP	200	−5.93 ± 3.62°C
	500	−8.24 ± 2.25°C
	1500	−14.22 ± 0.74°C
DTPMP	200	−12.72 ± 3.56°C
	500	−6.67 ± 6.79°C
	1500	−13.47 ± 2.20°C
PPA	200	−9.55 ± 3.83°C
	500	−8.52 ± 4.17°C
	750	−8.89 ± 7.96°C
HEDP	200	−10.97 ± 6.61°C
	500	−6.15 ± 7.49°C
	1500	−13.01 ± 1.71°C
Uramil–*N*,*N*-diacetic acid	200	−2.36 ± 2.69°C
	500	−4.69 ± 3.73°C
	1000	−6.10 ± 3.30°C
	1500	−7.50 ± 2.38°C

[a] Moles of additive per mole of LiBr (ppm).

To test this concept crystallization experiments were performed at various concentrations a_a of uramil–*N*,*N*-diacetic acid from 200 to 1500 ppm and other additives at various concentrations. The data are given in Table 4. Using this theoretical concept, the crystallization point due to surface nucleation as a function of the concentration of uramil–*N*,*N*-diacetic acid was predicted as shown in Fig. 6. As can be seen from the good fit of the experimental data we have a quantitative explanation of the crystallization point data, confirming the theoretical approach. Direct measurement of the adsorption isotherm of uramil–*N*,*N*-diacetic acid on LiBr · $2H_2O$ crystals was found to be too difficult experimentally for a host of reasons. The results of this fit for uramil–*N*,*N*-diacetic acid and those for other crystallization inhibitor additives are shown in Table 5.

TABLE 5

Γ_m^{-1}, the Adsorbed Area at Monolayer Coverage, and $K_{Langmuir}$, the Adsorption Equilibrium Constant for Various Crystallization Inhibitor Additives Derived from the Decrease in the Crystallization Temperature with Additive Concentration

Additive	Γ_m^{-1} (nm^2)	$K_{Langmuir}$ (ppm^{-1})
MDPA	0.65	10
PPA	0.65	10
ATMP	1.0	0.5
DTPMP	0.7	20
HEDP	0.7	20
Uramil–*N*,*N*-diacetic acid	1.0	0.09

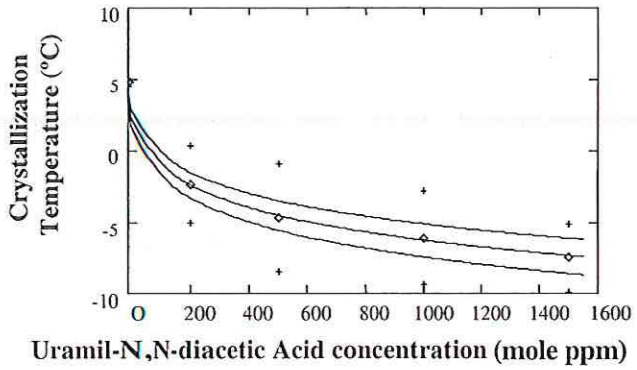

FIG. 6. Crystallization temperature (°C) as a function of uramil–*N*,*N*-diacetic acid concentration. Data points (◇) are experimental crystallization temperatures with ± standard deviation indicated with + symbols. The central curve is predicted using the Gibbs adsorption equation to calculate the interfacial energy, and the Langmuir adsorption isotherm with the monolayer adsorption density $\Gamma_m = 1$ nm^2 per adsorbed molecule and the adsorption equilibrium constant $K_{Langmuir} = 0.09$/ppm. The upper and lower curves use the same proceedure by over-and underpredicting the energy by 3% since that was the accuracy in the energy measured by best fit without additive. This suggests that there is another effect influencing the distribution of surface energy when the additive is present at the interface, as the experimental standard deviation is larger than the standard deviation of 3% depicted by the upper and lower curves.

As a result of knowing that additive adsorption plays a critical role in crystallization inhibition, we can now focus on what makes a molecule adsorb at the surface. In the Langmuir adsorption isotherm there are two parameters, the monolayer adsorption density Γ_m and the adsorption equilibrium constant $K_{Langmuir}$. The monolayer adsorption density is related to the surface area covered by one molecule and relates to the size of the molecule and the density of sites at the surface where the molecule can be attached. Using molecular modeling (19) we have modeled the $0\bar{1}0$ surface of LiBr · $2H_2O$ crystal and the energy-relaxed conformation of various additives at the surface of this crystal. This crystal surface has bound H_2O molecules exposed to the solution and in between and below them Li^+ and Br^- ions as seen in Fig. 7. Also shown in Fig. 7 are the sizes of MDPA and uramil–*N*,*N*-diacetic acid in their preferential binding sites, i.e., a wedge-like pocket in the crystal surface over a Li atom in the second layer of atoms in the crystal. Comparing, we can see that MDPA sits at essentially the same location as uramil–*N*,*N*-diacetic acid on the crystal surface due to the geometric similarity of the amine diphosphonic acid and the amine diacetic acid groups. However, the area occupied by uramil–*N*,*N*-diacetic acid (0.92 nm^2) covers slightly more than two of these sites, while MDPA (0.34 nm^2) covers one. This difference in surface monolayer coverage will have profound effects on the surface energy and the crystallization point of the LiBr solution with additive. As a result, we can put twice the number of molecules of MDPA on the surface as that of uramil–*N*,*N*-diacetic acid in a monolayer if they have equal effects on the surface energy. Also shown in Fig. 7 are plots of the interaction energy of the additive molecule either MDPA or uramil–*N*,*N*-diacetic acid with the surface at various locations (frames) at the surface. The lowest

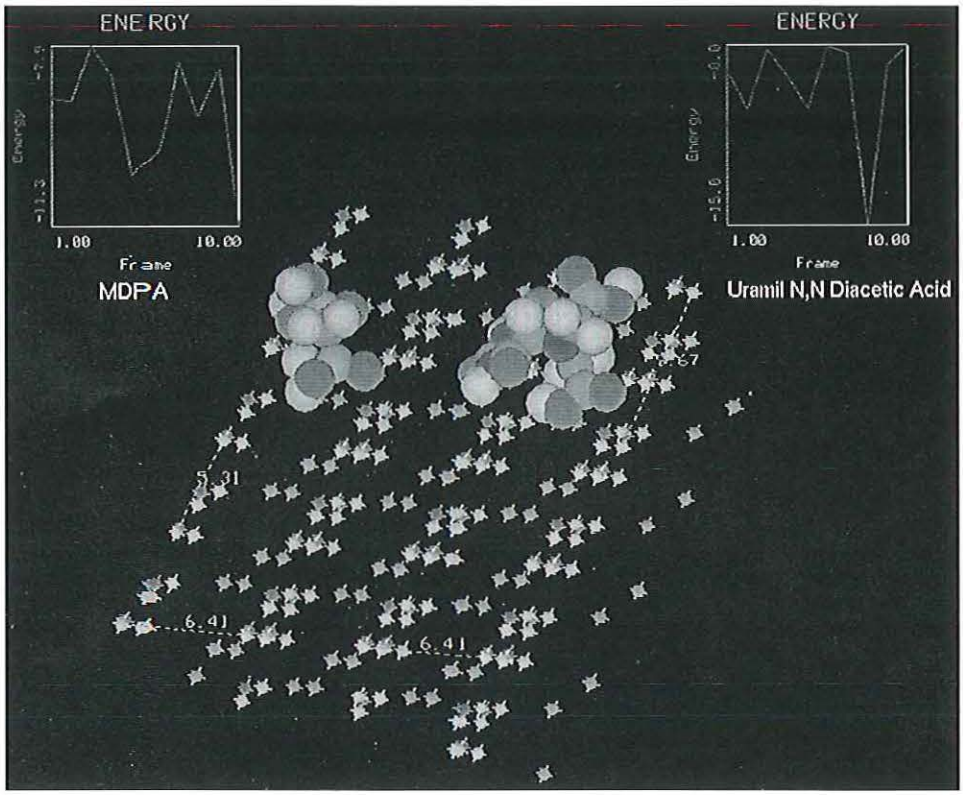

FIG. 7. Molecular modeling of MDPA and uramil–*N*,*N*-diacetic acid additives at the $0\bar{1}0$ surface of LiBr · 2H$_2$O crystal surface. The two graphs show the interaction energy of the additive with the crystal's surface as a function of location (frame). The lowest energy configuration of the adsorbed molecule is depicted at the surface.

energies of all the locations sampled, −11.5 kcal/mol for MDPA and −15.0 kcal/mol for uramil–*N*,*N*-diacetic acid, are the energies of relaxed structures in the absence of solvent molecules. But since uramil–*N*,*N*-diacetic acid sits on two sites, the per-site energy of MDPA is larger than that of uramil–*N*,*N*-diacetic acid, suggesting that K_{Langmuir} for MDPA is larger than that of uramil–*N*,*N*-diacetic acid. Both the absorbed conformation and interaction energy observations agree with the experimental observations that MDPA has been shown to have a crystallization temperature of -10.16 ± 3.17°C, while that of uramil–*N*,*N*-diacetic acid is -5.69 ± 2.92°C compared to a crystallization temperature of the same 60.54% LiBr solution without additive of $+3.30 \pm 0.44$°C. Comparing the molecular area of uramil–*N*,*N*-diacetic acid due to molecular modeling, 0.92 nm^2, with that obtained by the best fit of the crystallization point data as a function of uramil–*N*,*N*-diacetic acid concentration, 1 nm^2, we find very good agreement. At present, we have not found the algorithm that will allow prediction of the adsorption equilibrium constant K_{Langmuir} from molecular modeling calculation, but it is related to the energy calculations shown in Fig. 7.

Standard Deviation of Crystallization Temperature

It has been a curiosity that the standard deviation of the crystallization temperature with additive (±7.5°C for HEDP) is significantly larger than that without additive (±0.5°C), and both of these standard deviations are considerably larger than the precision (±0.01°C) of the thermocouples employed to measure the crystallization temperature. The increase in standard deviation is not linked to the 3% error in the surface energy determined without additives (see Fig. 6) but to a larger value of approximately 8%. The increase in standard deviation appears to be linked with the additives, which are good crystallization inhibitors, (see Table 2). This increase in standard deviation is believed to be due to the nonuniform adsorbed surface coverage by the additive, as shown schematically in Fig. 8. High and low surface coverage in the form of patches is a common phenomenon observed with adsorption from solution (20). Using the crystallization temperature data, we can determine the distribution of surface energies (or surface coverage). Each of the crystallization temperature measurements is indicative of the site at the surface where the first nucleus was formed, leading to rampant heterogeneous nucleation. Multiple measurements thus probe different parts of the surface with their individual surface energies. Assembling the crystallization temperature data in descending order and determining the cumulative probability associated with each measurement allow the prediction of the fractional surface coverage associated with the surface energy of each particular crystallization temperature measurement in the distribution. For uramil–*N*,*N*-diacetic acid, the distribution of

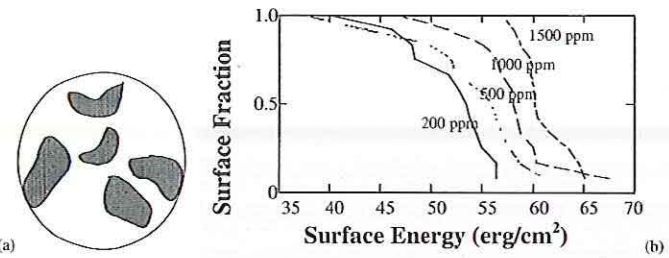

FIG. 8. (a) Schematic of surface coverage after patchwise adsorption of additive giving an average surface coverage corresponding to $\Gamma_a^{(1)}$. (b) Distribution of surface energies as determined by the repeated crystallization point measurements of samples with various concentrations of uramil–*N*,*N*-diacetic acid.

surface coverage has been determined by this method and is given in Fig. 8.

CONCLUSIONS

The effects of additives at concentrations of 250–1500 ppm on the LiBr crystallization temperature have been studied. Some of these additives further decreased the crystallization temperature by up to 13°C below the experimental crystallization temperature and up to 22°C below the equilibrium solubility of the same solution without additive. These additives are described as crystallization inhibitors. Large decreases in the crystallization temperature can be correlated with large values of complexation constants of the additive for either the Li^+ or the Br^- ion in solution. Solution complexation, however, is not sufficient itself to explain the magnitude of the decrease in the crystallization temperature. This decrease of the crystallization temperature is quantitatively justified by the additive adsorption at the crystal/solution interface, altering the surface energy.

ACKNOWLEDGMENTS

This project was sponsored by the Gas Research Institute under Contract No. 5094-260-2895. N.J. thanks the "Stiftung Entwicklungsfond Seltene Metalle" (Switzerland) for a scholarship, the Commission for Educational Exchange between the United States, Belgium, and Luxembourg for a Fulbright Award, and the North Atlantic Treaty Organization for a scholarship.

REFERENCES

1. Aphornratan, S., and Eames, I. W., *Int. J. Refrig.* **18,** 244 (1995).
2. Smith, J. M., and Van Ness, H. C., "Introduction to Chemical Engineering Thermodynamics," 2nd ed. McGraw-Hill, New York, 1959.
3. Duvall, K. N., Dirksen, J. A., and Ring, T. A., *J. Colloid Interface Sci.* **240** (2001).
4. Sarig, S., and Kahana, F., *J. Cryst. Growth* **35,** 145 (1976).
5. Nyvlt, J., and Ulrich, J., "Admixtures in Crystallization." VCH Weinheim, Germany, 1995.
6. Brecevic, L., and Furedi-Milhofer, H., *in* "Industrial Crystallization" (J. W. Mullin, Ed.), p. 277. Plenum, New York, 1976.
7. Brit. Pat. 1,126,615 (1968).
8. Buckley, H. E., *Z. Krist.* **81,** 157 (1932).
9. Buckley, H. E., *Z. Krist.* **82,** 37 (1932).
10. Myerson, A. S., Green, D. A., and Meenan, P., Eds., "Crystal Growth of Organic Materials," ACS Conf. Proc. Ser. Am. Chem. Soc., Washington, DC, 1996.
11. Niehorster, S., Henning, S., and Ulrich, J., *in* "Crystal Growth of Organic Materials" (A. S. Meyerson, D. A. Green, and P. Meenan, Eds.), ACS Conf. Proc. Ser., p. 58. Am. Chem. Soc., Washington, DC, 1996.
12. Sun, W.-M., and Myerson, A. S., *in* "Crystal Growth of Organic Materials" (A. S. Meyerson, D. A. Green, and P. Meenan, Eds.), ACS Conf. Proc Ser., p. 249. Am. Chem. Soc. Washington, DC, 1996.
13. Zaltash, A., and Ally, M. R., *J. Chem. Eng. Data* **37,** 110 (1992).
14. National Research Council, "International Critical Tables" (E. W. Washbum, Ed.), Vol. III, p. 727. McGraw-Hill, New York, 1928.
15. Broul, M., Nyyvlt, J., and Sohnel, O., "Solubility in Inorganic Two-Componet Systems," Physical sciences data 6. Elsevier, Amsterdam, 1981.
16. Adamson, A. W., "Physical Chemistry of Surfaces," 4th Ed., p. 322. Wiley, New York, 1982.
17. Yao, *et. al.*, *J. Chem. Eng. Data* **36,** 96 (1991).
18. Gibbs, J. W., "The Collected Works of J. W. Gibbs," Vol. I, p. 219. Longmans, Green, New York, 1931.
19. BioSym Solids Docking software from Molecular Simulations Inc. (MSI).
20. Guo, L.-C., Zhang, Y., and Uematsu, K., *J. Am. Ceram. Soc.*, to be published.
21. Martell, A. E., and Smith, R. M., "Critical Stability Constants 1." Plenum, New York, 1974.
22. Smith, R. M., and Martell, A. E., "Critical Stability Constants 2." Plenum, New York, 1974.
23. Smith, R. M., and Martell, A. E., "Critical Stability Constants 3." Plenum, New York, 1974.
24. Smith, R. M., and Martell, A. E., "Critical Stability Constants 4." Plenum, New York, 1976.
25. Smith, R. M., and Martell, A. E., "Critical Stability Constants 5." Plenum, New York, 1982.
26. Smith, R. M., and Martell, A. E., "Critical Stability Constants 6." Plenum, New York, 1989.
27. Perrin, D. D., "Stability Constants of Metal-Ion Complexes. Part B Organic Ligands." Oxford, Pergamon, New York, 1979.
28. He, S., Kan, A. T., and Tomson, M. B., *in* Water Soluble Polymers—Solution Properties and Applications" (Z. Amjad, Ed.), pp. 163–171. Plenum, New York, 1998.
29. Ferguson, R. J., "Developing Scale Inhibitor Dosage Models," available at www.frenchcreeksoftware.com/wt92.htm, 1/14/99; *Ind. Water Treat Mag.*, to be published.